Symmetry of phonon, magnetic, and spin-phonon excitations in $GdSr_2RuCu_2O_8$ single crystals

V. G. Hadjiev,[1] J. Bäckström,[2] V. N. Popov,[3] M. N. Iliev,[1] R. L. Meng,[1] Y. Y. Xue,[1] and C. W. Chu[1,4]
[1]*Texas Center for Superconductivity, University of Houston, Houston, Texas 77204-5932*
[2]*Department of Applied Physics, Chalmers University of Technology and Göteborg University, SE 41296 Göteborg, Sweden*
[3]*Faculty of Physics, University of Sofia, BG 1126 Sofia, Bulgaria*
[4]*Lawrence Berkeley National Laboratory, 1 Cyclotron Road, Berkeley, California 94720*
(Received 2 March 2001; published 12 September 2001)

We present a polarized Raman scattering study of $GdSr_2RuCu_2O_8$ single crystals. In this compound, the RuO_6 octahedra are rotated around the c axis that in turn gives some Raman activity of the oxygen (O_{Ru}) vibrations at 265 cm^{-1} (A_{1g}), 411 cm^{-1} (B_{2g}) and 607 cm^{-1} (B_{1g}). These vibrations, as well as those of the apical oxygen of RuO_6 at 654 cm^{-1} (A_{1g}) and the Cu-plane oxygen at 318 cm^{-1} (B_{2g}), clearly respond to the onset of magnetic ordering at $T_m \approx 140$ K. In particular, the 265 cm^{-1} mode hardens anomalously with decreasing temperature below T_m. Notably, the corresponding phonon line is absent in the Raman spectra of $GdSr_2NbCu_2O_8$ (Nb^{5+}:$4d^0$), a compound isomorphic to $GdSr_2RuCu_2O_8$ (Ru^{5+}:$4d^3$). We argue that the eigenvector of the 265 cm^{-1} phonon (rotational mode) facilitates efficient modulation of the Ru(t_{1g})-O_{Ru}(p) bands. This modulation gives both Raman scattering strength to the 265 cm^{-1} mode and strong spin-phonon coupling.

DOI: 10.1103/PhysRevB.64.134304 PACS number(s): 63.20.Ls, 74.70.−b, 78.30.Hv, 71.70.−d

I. INTRODUCTION

Recent studies of ruthenate-cuprates have demonstrated the rather peculiar properties of these materials.[1–5] For instance, earlier suggestions[1,2] that superconducting $GdSr_2RuCu_2O_8$ is also ferromagnetically ordered have been challenged by neutron powder diffraction experiments[3,4] where no sign of ferromagnetism has been found. Instead, G-type antiferromagnetic (AFM) order of Ru moments has been evidenced below $T_m = 138$ K.[4] On the other hand, magnetic measurements of $GdSr_2RuCu_2O_8$ have clearly demonstrated spontaneous magnetization below T_m,[2,5] that is, an existence of a ferromagnetic (FM) component of magnetic ordering. It is, however, unclear whether this ferromagnetic component stems from a canted AFM structure or spatially separated AFM and FM phases. It is believed that ferromagnetic excitations have also been detected by Raman spectroscopy[6,7] as a magnonlike peak (hereafter called the magnetic peak) at ~ 150 cm^{-1}. This peak has also been observed in other compounds closely related to $GdSr_2RuCu_2O_8$.[8] The behavior of the position and intensity of the magnetic peak under applied magnetic field is similar to that one when decreasing the temperature,[8] which gives further support to a ferromagnetic origin. The Raman intensity of the magnetic peak varies in different $GdSr_2RuCu_2O_8$ samples and can be very weak or even vanishing.[9] The Raman response of $GdSr_2RuCu_2O_8$ seems to be strongly influenced by crystalline morphology that is featured with fine granularity, heavy twinning, a variety of domains, and domain boundaries.[10] Interestingly, the Raman spectra of polycrystalline $GdSr_2RuCu_2O_8$ reported so far have been mostly unpolarized[6–9,11] albeit micron-size grains were probed.[6,9]

In this paper we present a Raman scattering study performed on nonsuperconducting $GdSr_2RuCu_2O_8$ single crystals. We measured the polarized Raman spectra of $GdSr_2RuCu_2O_8$ in several exact configurations that allowed us to determine the symmetries of the phonon and coupled spin-phonon excitations. For comparison, we also recorded the Raman spectra of isomorphic[12] $GdSr_2NbCu_2O_8$. We find essential differences between the two compounds that reveal the unique role of Ru in formation of magnetic moments, ordering, and doping of $GdSr_2RuCu_2O_8$.

II. EXPERIMENT

In the Raman experiment, we measured small $GdSr_2RuCu_2O_8$ single crystals with rectangular faces of $\sim 30 \times 30$ μm^2 in size, embedded in a matrix of reaction residuals. The crystals were grown from CuO flux. First, presintered powders of $GdSr_2RuCu_2O_8$ and CuO with a molar ratio of 3/7 were thoroughly mixed. The mixture was put into a 30-ml Pt crucible, placed in a muffle furnace, and heated up to 1150°C in air at a rate of 15°C/h to ensure a homogeneous melting, and held for 15 h. In addition, a polycrystalline $GdSr_2NbCu_2O_8$ sample was prepared by solid-state reaction of stoichiometric powders of NbO_2, $SrCO_3$, Gd_2O_3, and CuO as described in Ref. 5.

Figure 1 displays the results of magnetic measurements of a $GdSr_2RuCu_2O_8$ sample consisting of a bunch of single crystals. The temperature dependence of magnetization reveals a relatively broad magnetic transition at $T_m \approx 140$ K [defined as the inflection point of the field-cooled (FC) magnetization] and no indication of superconductivity at low temperatures. The increase of magnetization at very low temperatures is due to the antiferromagnetic ordering of Gd moments at 2.8 K.[13] The deviation of FC magnetization from the zero-field cooled (ZFC) one persists up to 300 K, which may be due to minor phases between the crystals in the sample.

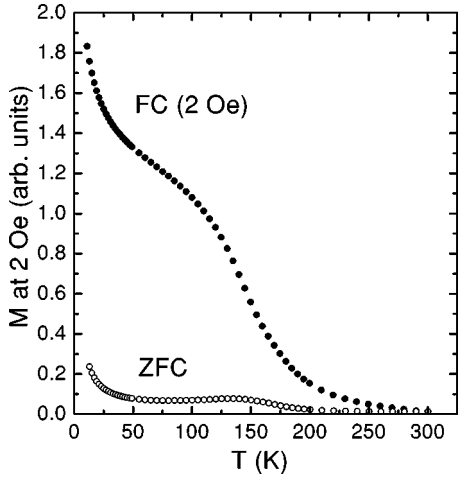

FIG. 1. Temperature dependence of magnetization of $GdSr_2RuCu_2O_8$ single crystals in zero-field cooled (ZFC) and field-cooled (FC at 2 Oe) regimes.

The Raman spectra were recorded using a notch-filter-equipped single-grating spectrometer with a liquid-nitrogen-cooled charge-coupled device detector. The 514.5-nm Ar^+ ion laser line was used for excitation of the samples using a microprobe attachment with a $\times 50$ objective for focusing the incoming beam on a spot of ≈ 2 μm in diameter and collecting the scattered light. The samples were attached to the cold finger of a helium microcryostat, held at different temperatures, and measured in backscattering geometry. We denote the scattering configurations in the Porto notation $i(kl)m$, where i and m stand for the propagation direction of the incident and scattered photons, while k and l represent their polarization, respectively. The symbols x,y, and z denote directions parallel to the a, b, and c axes of the crystal, respectively, and x' and y' are two mutually orthogonal directions along $[110]$ and $[1\bar{1}0]$.

III. EXPERIMENTAL RESULTS AND DISCUSSION

A. Symmetry analysis and lattice dynamics calculations

The crystal structure of $GdSr_2RuCu_2O_8$ can be derived from the tetragonal ($P4/mmm$) $GdBa_2Cu_3O_6$ structure by substituting the basal plane Cu for Ru and Ba for Sr, and filling up the oxygen sites in the Ru plane. Thus formed RuO_6 octahedra (Ru, 4 O_{Ru}, and two apical oxygen O_a atoms) are rotated around the c axis by $\approx 14°$ to match the in-plane Ru-O_{Ru} bonds with the shorter Cu-O_{Cu} ones in the CuO_2 planes.[3] This rotation is facilitated by smaller ionic radius of Sr than that of Ba. The rotational displacements of O_{Ru} lead to doubling of the unit cell and change of the space group according to $P4/mmm(a,a,c) \rightarrow P4/mbm(a\sqrt{2},a\sqrt{2},c)$,[3] where a and c are the lattice constants. The doubling of the unit cell increases the number of the Raman-active phonons from 10 ($4A_{1g}+B_{1g}+5E_g$, $P4/mmm$) to 22 ($6A_{1g}+2B_{1g}+4B_{2g}+10E_g$, $P4/mbm$).[9] The Raman intensity of the E_g phonons is usually very weak, and a doubling of the unit cell is expected to mostly add new lines of A_{1g}, B_{1g}, and B_{2g} symmetry in the Raman spectra. The additional two A_{1g} modes in the $P4/mbm$ structure correspond to rotational motion of the RuO_6 octahedra and the CuO_5 pyramides around the c axis, respectively. These modes should have vanishing frequency in $P4/mmm$, that is, they are soft modes for the transition $P4/mmm \rightarrow P4/mbm$. We also note that this structural transition transforms the B_{1g} mode in $P4/mmm$, that involves the out-of-phase vibrations of O_{Cu}, to a B_{2g} mode in $P4/mbm$.

TABLE I. Shell model parameters for $GdSr_2RuCu_2O_8$.

Ion	$Z(\|e\|)$	$Y(\|e\|)$	α(Å^3)	Ionic pair	a(eV)	b(Å^{-1})	c(eVÅ^6)
Ru	4.75	1.4	0.0	Ru-O	3900	3.565	0
Sr	1.90	3.0	2.5	Sr-O	888	2.536	0
Gd	2.85	1.7	0.7	Gd-O	1631	2.854	0
Cu	1.90	3.0	1.3	Cu-O	1600	3.476	0
O	-1.90	-3.0	3.0	O-O	22764	6.711	20.37

The Γ-point phonons were calculated using a shell model with model parameters taken from studies of a number of perovskite-like compounds.[14] In this model the interionic interactions are described by long-range Coulomb potentials and short-range Born-Mayer potentials of the form $V = a\exp(-br) - c/r^6$ with r being the interionic separation. The polarizability of the ions is accounted for in the dipole approximation representing each ion as a point-charged core coupled with a force constant k to a massless shell with charge Y surrounding it so that the free ionic polarizability α is given by $\alpha = Y^2/k$. The values of the shell model parameters used in the present calculation are given in Table I.

B. Phonons

In Fig. 2 we present the low-temperature Raman spectra of (a) $GdSr_2RuCu_2O_8$ single crystals, measured for various scattering configurations, and (b) polycrystalline $GdSr_2NbCu_2O_8$. The Raman selection rules for tetragonal groups assert that $y'(zz)\bar{y'}$ selects spectral components of A_{1g} symmetry, $y'(x'x')\bar{y'} \rightarrow A_{1g}+B_{2g}$, $z(x'x')\bar{z} \rightarrow A_{1g}+B_{2g}$, $z(xx)\bar{z} \rightarrow A_{1g}+B_{1g}$, $z(xy)\bar{z} \rightarrow A_{2g}+B_{2g}$, $z(x'y')\bar{z} \rightarrow A_{2g}+B_{1g}$, and $y'(xz)\bar{y'} \rightarrow E_g$. The A_{2g} phonons are not Raman active in $P4/mbm$. From Fig. 2(a) follows that the excitations at 158, 275, 439, and 654 cm^{-1} are of A_{1g} symmetry, those at 318 and 411 cm^{-1} are B_{2g}, and the one at 608 cm^{-1} is of B_{1g} symmetry. We assign the line at 158 cm^{-1} to a superposition of the two A_{1g} modes involving Cu and Sr vibrations along the c axis. This assignment is consistent with the results of the lattice dynamical calculations given in Table II. Additional support is found in the spectrum in Fig. 2(b), where somewhat different interatomic distances[12] in $GdSr_2NbCu_2O_8$ lead to better resolved separation of the Cu and Sr modes. The A_{1g} modes at 318 and 439 cm^{-1} in Fig. 2(a) correspond to the out-of-phase and in-phase O_{Cu} vibrations along the c axis, respectively. The $A_{1g}(O_a)$ vibration appears at 654 cm^{-1}.

The three A_{1g} vibrations along the c axis in $GdSr_2NbCu_2O_8$ are easily identified in the spectrum in Fig.

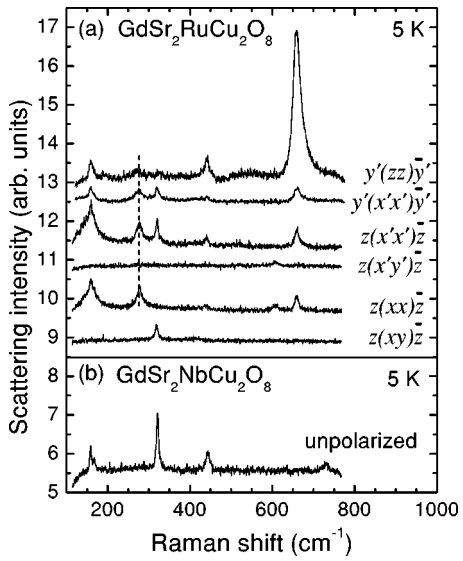

FIG. 2. Polarized Raman spectra of (a) $GdSr_2RuCu_2O_8$ single crystals and (b) polycrystalline $GdSr_2NbCu_2O_8$ at 5 K. All the polarization configurations are given in (a) except for the $y(zx)y$ (E_g) one for which no phonon peaks have been detected. The upper two spectra in (a) are taken from one and the same crystal, and the bottom four from another one.

2(b) at 331, 444, and 732 cm^{-1}. The higher frequency of the O_a mode in $GdSr_2NbCu_2O_8$ is due to the shorter $d_{O_a\text{-}Nb}=1.856$ Å bondlength[12] compared to $d_{O_a\text{-}Ru}=1.914$ Å in $GdSr_2RuCu_2O_8$.[3] It is well established that the corresponding O_a-Cu(chain) bondlength in $RBa_2Cu_3O_7$ (R is rare earth) controls the A_{1g} apical oxygen frequency.[15] A simple model[16] for oxygen vibrations in cuprates gives that the square of the apical oxygen frequency $\omega^2_{O_a}$ varies with the valence of the cation Z_{Me} and the metal-oxygen distance as $Z_{Me}\ d^{-3}_{O_a\text{-}Me}$ due to the change of ionic binding energy. A straightforward comparison gives that the ratio of experimentally measured frequencies $\omega^2_{O_a\text{-}Ru}/\omega^2_{O_a\text{-}Nb}$ agrees well with $Z_{Ru}\ d^{-3}_{O_a\text{-}Ru}/Z_{Nb}\ d^{-3}_{O_a\text{-}Nb}$ provided $Z_{Nb}=+5$ and $Z_{Ru}\approx +4.3$. Interestingly, this particular valence of Ru corroborates well that obtained from the valence bond sum in $GdSr_2RuCu_2O_8$.[10]

Table II summarizes the experimentally measured phonon frequencies and those predicted by lattice dynamical calculations. Four of the A_{1g} modes and one B_{2g} mode are clearly seen in the Raman spectra of both the Ru- and the Nb-based compounds. From Table II it follows that these modes include predominantly vibrations along the c axis. On the other hand, the phonons at 275 (A_{1g}), 411 (B_{2g}) and 607 (B_{1g}) cm^{-1} in the spectra of $GdSr_2RuCu_2O_8$ have no counterpart in the spectra of $GdSr_2NbCu_2O_8$. We note that all these phonons involve O_{Ru} vibrations.

C. Magnetic excitations

An interesting Raman feature is the relatively broad peak at ~ 150 cm^{-1} in the $z(xx)\bar{z}$ and $z(x'x')\bar{z}$ spectra at 5 K in Fig. 2(a). This peak resembles the magnetic peak in $GdSr_2RuCu_2O_8$ reported in Refs. 6–8, but has much lower intensity. In addition, the spectral weight of the 150 cm^{-1} peak rapidly decreases with increasing temperature, and we were not able to follow the temperature dependence previously observed[6–8] in polycrystalline samples. On the other hand, the shape and position of the 150 cm^{-1} peak, as well as the fact that it appears below T_m, are much in favor of the magnetic peak assignment. Despite these uncertainties it is tempting to describe the peculiar symmetry properties of the 150 cm^{-1} peak. From the spectra in Fig. 2(a) it follows that the magnetic peak in $GdSr_2RuCu_2O_8$ has A_{1g} symmetry, a rather unusual symmetry for Raman-active magnetic excitations. Raman scattering from magnons proceeds predominantly through spin-orbit interaction.[17] Creation of a magnon in the Raman process requires a spin-flip in the intermediate state that rotates the scattered light polarization by 90°, that is, magnons are usually seen for crossed incident and scattered light polarizations. The latter property excludes the A_{1g}

TABLE II. Experimental and calculated Raman phonon mode frequencies of $GdSr_2RuCu_2O_8$ within the $P4/mbm$ space group.

Mode	Experiment (5 K)	Calculations (shell model)	Atomic motions
$A_{1g}(1)$	158	176	Cu stretching vibration along the c axis
$A_{1g}(2)$	158+	186	Sr stretching vibration along the c axis
$A_{1g}(3)$		256	Rotation of CuO_5 around the c axis
$A_{1g}(4)$	275	323	Rotation of RuO_6 around the c axis
$A_{1g}(5)$	439	448	In-phase vibrations of O_{Cu} along the c axis
$A_{1g}(6)$	659	644	O_a stretching vibration along the c axis
$B_{1g}(1)$		497	In-plane antistretching vibrations of O_{Cu}
$B_{1g}(2)$	607	688	In-plane antistretching vibrations of O_{Ru}
$B_{2g}(1)$		178	Sr Along the c axis
$B_{2g}(2)$	320	297	Out-of-phase vibrations of O_{Cu} along the c axis
$B_{2g}(3)$	411	425	''Scissors'' type, in-plane O_{Ru} vibrations
$B_{2g}(4)$		488	''Scissors'' type, in-plane O_{Cu} vibrations

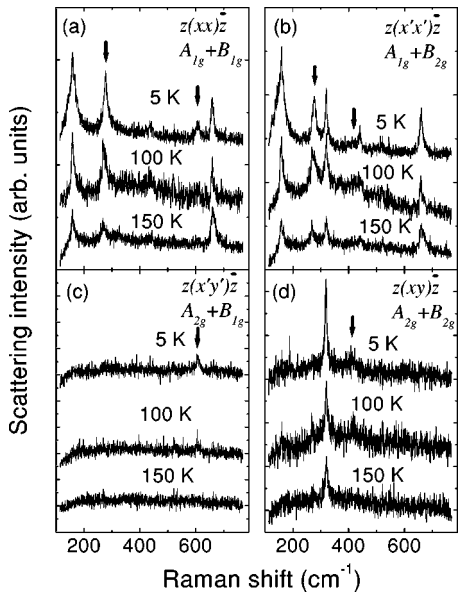

FIG. 3. In-plane polarized Raman spectra of $GdSr_2RuCu_2O_8$ single crystals for three different temperatures. The arrows denote the position of the O_{Ru} modes. Note that the Raman lines strictly obey the selection rules and have exact symmetry.

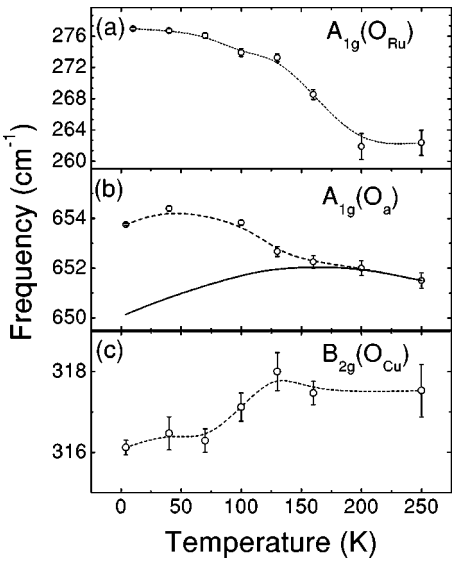

FIG. 4. Temperature dependence of (a) the $A_{1g}(O_{Ru})$, (b) $A_{1g}(O_a)$, and (c) $B_{2g}(O_{Cu})$ modes in $GdSr_2RuCu_2O_8$. The solid line in (b) shows the calculated dependence of the O_a frequency ω_{latt} with temperature without spin-phonon coupling (details given in II D).

symmetry. In addition, this peak is absent in the $y'(x'x')\bar{y}'$ spectrum in Fig. 2(a). This suggests that either the Raman scattering from magnetic excitations at $\sim 150\ \mathrm{cm}^{-1}$ also depends on the **k**-vector direction of the exciting light or that the two crystals characterized by the $y'(x'x')\bar{y}'$ and $z(x'x')\bar{z}$ spectra are different. Unfortunately, the reason for the magnetic-peak-intensity variation in $GdSr_2RuCu_2O_8$ between different samples remains still unclear. More experimental studies on samples with diverse crystalline morphology are needed to clarify the origin of the 150 cm^{-1} excitation.

D. Phonon anomalies correlated with the magnetic transition

Coupling of phonons to magnetic excitations in solids results in phonon self-energy, that is, the frequency and linewidth of the phonons change due to interaction. Magnetic ordering can also influence the phonon self-energy by a variety of mechanisms known as spin-dependent phonon Raman scattering.[18,19] Usually these effects manifest themselves in a peculiar behavior of phonon frequency or intensity near or below T_m.

Figure 3 displays the Raman spectra of $GdSr_2RuCu_2O_8$ measured at temperatures slightly above and below T_m. Close examination of the temperature dependence of phonon frequency suggests that at least three of the phonons show anomalous behavior below T_m. Two of these phonons (264 cm^{-1} and 652 cm^{-1}) involve oxygen vibrations of RuO_6 and one (318 cm^{-1}) of CuO_2 planes. Their frequencies as a function of temperature are shown in Fig. 4. The 264 cm^{-1} mode frequency shifts strongly upward to 275 cm^{-1} at 5 K [Fig. 4(a)] in a manner that resembles the temperature dependence of the field-cooled magnetization (Fig. 1). Similar behavior has also been observed in polycrystalline $GdSr_2RuCu_2O_8$ samples.[6–9] We discuss this in more detail in Sec. II E.

The temperature dependence of the $A_{1g}(O_a)$ mode frequency in Fig. 4(b) looks at a first glance typical of a phonon in a shrinking lattice as that of $GdSr_2RuCu_2O_8$.[3] However, we note that the neutron diffraction study by Chmaissem *et al.* indicated that the O_a-Ru bondlength $d_{O_a\text{-Ru}}$ increases with decreasing temperature.[3] If this is the case, the frequency of the O_a mode should decrease with temperature according to $\omega_{O_a} \propto d_{O_a\text{-}Ru}^{-3/2}$ (see, e.g., Sec. II B) unless other mechanisms contribute to the real part of the phonon self-energy (i.e., frequency). The solid curve in Fig. 4(b) is a fit of $\omega_{latt} = a d_{O_a\text{-Ru}}^{-3/2} + b(N_{\omega_{latt}} + \frac{1}{2})$ (a and b are parameters) to the frequencies measured in the paramagnetic region. The first term accounts for the frequency change due to the altered ionic binding energy resulting from the varying bond length. The second term, where $N_{\omega_{latt}} = 1/[\exp(\hbar\omega_{latt}/2k_B\mathrm{T}) - 1]$, gives the contribution from the anharmonic two-phonon decay process. In other words, the solid curve in Fig. 4(b) shows the expected temperature dependence of the O_a phonon frequency based on the bondlength data in Ref. 3 and our measured high-temperature phonon frequencies. Clearly, they do not agree when $T < T_m$, suggesting the existence of a spin-phonon interaction contribution to the real part of the $A_{1g}(O_a)$ phonon self-energy.

The 320 cm^{-1} B_{2g} mode frequency versus temperature is given in Fig. 4(c). It shows a nonmonotonous behavior and an abrupt softening below T_m. At the end, we note the implication of these observations: oxygen atoms mediate magnetic interactions in $GdSr_2RuCu_2O_8$ and can in principle be used to probe the magnetic ordering.

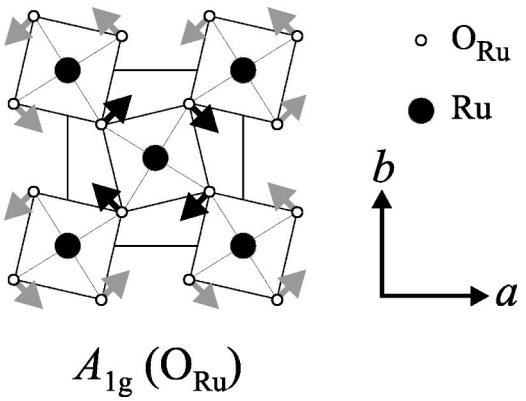

FIG. 5. Eigenvector of the $A_{1g}(O_{Ru})$ mode derived from LDC shell model calculations. The open and solid circles denote O_{Ru} and Ru atoms, respectively. The mode symmetry is given for the $P4/mbm$ group.

An example of apparent spin-dependent phonon Raman scattering in $GdSr_2RuCu_2O_8$ is demonstrated by the 411 cm^{-1} (B_{2g}) and 607 cm^{-1} (B_{1g}) phonons. These lines become observable below T_m and their Raman intensity increases further with decreasing temperature. The enhancement of Raman intensity of the two phonons is evidence for a spin-dependent scattering mechanism.[19] In a magnetically ordered phase, the Raman intensity changes with temperature as $I_{ph}(T) \propto |R_{ph} + M\langle \mathbf{S}_0 \cdot \mathbf{S}_{nn}\rangle / S^2|^2$,[19] where $\langle \mathbf{S}_0 \cdot \mathbf{S}_{nn}\rangle / S^2$ is the nearest-neighbor spin correlation function and R_{ph} is the spin-independent phonon Raman amplitude. This equation is valid for both ferromagnetic and antiferromagnetic magnetic ordering. The type of magnetic ordering reflects only on the sign of M, provided the vertices are real, being opposite for the two types of ordering. Our experiment shows that the Raman intensity of the 411 cm^{-1} and 607 cm^{-1} lines is vanishing above T_m, that is, $I_{ph}(T > T_m) \propto R_{ph}^2 \approx 0$, and therefore $I(T < T_m) \propto |M\langle \mathbf{S}_0 \cdot \mathbf{S}_{nn}\rangle / S^2|^2$. We point out that $I_{ph}(T)$ of the 411 cm^{-1} and 607 cm^{-1} phonons in $GdSr_2RuCu_2O_8$ alone cannot distinguish to which of the magnetic ordering components the two phonons couple.

E. Phonon renormalization due to interaction with magnetic excitations

It is essential for the magnetic-order-dependent phonon self-energy effects that the phonon modulates those electronic bands that take part in formation of magnetic moments and the spin-spin coupling constants (exchange interaction). The effectiveness of this modulation depends on the phonon eigenvector. In Fig. 5 we display the eigenvectors of the 265 cm^{-1} (A_{1g}) phonon obtained by symmetry considerations and lattice dynamics calculations (LDC). The oxygen displacements in this mode are similar to those of the RuO_6 rotation that causes the $P4/mmm$ to $P4/mbm$ structural transition. First-principles electronic and magnetic structure calculations[20] for $GdSr_2RuCu_2O_8$ show that this rotation results in significant narrowing of the $4d$-electron bands that drives the system to AFM order. Indeed, an earlier calculation[21] within the $P4/mmm$ structure (without RuO_6 rotations) of the same compound has given FM ground state. In the FM ordered $P4/mmm$ phase the Ru-O_{Ru} hybridized bands, in particular Ru d_{xy}-O_{Ru} $p_{x(y)}$, strongly contribute to the density of states (DOS) at the Fermi energy (E_f), which gives itinerant character of Ru magnetism. A comparison with the DOS of the FM-$P4/mbm$ phase[21] shows that the RuO_6 rotation leads to more localized majority spin $d^{\uparrow}_{xy}$ states dipped below E_f, and depleted $d^{\uparrow}_{xy}$-$p_{x(y)}$ hybridization channel at E_f, that is, much less itinerant character of ferromagnetism. The FM ordering of Ru moments in $P4/mbm$ $GdSr_2RuCu_2O_8$, however, has been found energetically less favored than AFM.[20] In the AFM-$P4/mbm$ phase the more localized $d^{\uparrow}_{xy}$ and $d^{\uparrow}_{xz(yz)}$ states of a given Ru hybridize with the $d^{\downarrow}_{xy}$ and $d^{\downarrow}_{xz(yz)}$ states on the nearest-neighbor Ru sites through O_{Ru}. Therefore, the spin-spin coupling is carried through the superexchange mechanism. Interestingly, a soft mode similar to that at 265 cm^{-1} in $GdSr_2RuCu_2O_8$ has been found to freeze at the surface of the Sr_2RuO_4 superconductor and stabilize the FM fluctuations in the surface layer.[22] On the other hand, Mazin and Singh[23] have given an example in which the in-plane RuO_6 rotation in Sr_2YRuO_6 is coupled to AFM ordered Ru spins. In this compound the RuO_6 octahedra do not share common oxygen atoms. For these RuO_6 clusters the authors of Ref. 23 predict that a RuO_6 rotational mode with frequency of $\approx$270 cm^{-1} couples to magnetic excitations that flip the spin (magnons) of a RuO_6 cluster. From the above analysis we conclude that whatever type of magnetic ordering is established in $GdSr_2RuCu_2O_8$ the A_{1g} mode at 265 cm^{-1} should couple strongly to the magnetic excitations either through strong modulation of the d_{xy}-$p_{x(y)}$ bands in the FM phase or by perturbing the superexchange path in the AFM phase.

F. Raman scattering intensity of the 265 cm^{-1} mode

At the end we discuss the origin of the 265 cm^{-1} mode Raman intensity. The band structure calculations[20] of AFM-$GdSr_2RuCu_2O_8$ give that three bands cross the Fermi surface. These are a Ru-O_{Ru} bands derived from the antibonding $dp\pi$:d_{xy}-$p_{x(y)}$ orbitals and two Cu-O_{Cu} bands with $dp\sigma$:$d_{x^2-y^2}$-$p_{x(y)}$ character, as those in bilayer cuprates. In a FM ordered structure a fourth band, namely that of the $d_{xz(yz)}$-p_z orbitals, also crosses E_f. In view of the weak 265 cm^{-1} peak spectral weight, we suggest that it gains $xx(yy)$ Raman intensity from transitions between the Ru(d_{xy})-O_{Ru}($p_{x(y)}$) and Ru($d_{x^2-y^2}$)-O_{Ru}($p_{x(y)}$) bands, that is, transitions without charge transfer. Within the crystal-field approximation of $Ru^{5+}(4d^3)$, these transitions correspond to the $^4A_{2g} \rightarrow {}^4T_{2g}$ or $^4T_{1g}$ spin-allowed but parity-forbidden intraionic transitions that have relatively weak oscillator strength.[24] The Raman scattering is expected to be under resonance due to the energy gap of $\approx$2.5 eV between the two Ru-O_{Ru} bands.[20] Indeed, a preliminary resonance study of $GdSr_2RuCu_2O_8$[25] has found an enhancement of the 265 cm^{-1} phonon intensity by increasing the excitation laser energy from 1.92 eV to 2.41 eV. The $xx(yy)$-Raman intensity of the modes that involve Cu and O_{Cu} vibrations most likely comes from Cu(d_{xy})-O_{Cu}($p_{x(y)}$) $\rightarrow$Cu($d_{x^2-y^2}$)-O_{Cu}($p_{x(y)}$) transitions similar to those in

$YBa_2Cu_3O_7$.[26] Interestingly, the Raman spectrum of $GdSr_2NbCu_2O_8$ resembles more closely that of $YBa_2Cu_3O_6$, a fact that is consistent with insulating character of this compound.[12] In $GdSr_2NbCu_2O_8$ (Nb^{5+}:$4d^0$) the Nb($4d$)-O_{Nb} bands are empty. Therefore, the Nb($4d$)-O_{Nb} band-to-band transitions that give strength to the $xx(yy)$ Raman intensity of the rotational mode are not available anymore and the process is off resonance. We believe that this most likely is the reason for the vanishing intensity of the rotational mode in $GdSr_2NbCu_2O_8$.

IV. CONCLUSIONS

We have determined the symmetry of the phonon, magnetic, and coupled magnetic-phonon excitations in $GdSr_2RuCu_2O_8$ from polarized Raman spectra of single-crystal samples. Spin-phonon interactions are found to produce phonon self-energy effects for all the Raman-active oxygen vibrations in $GdSr_2RuCu_2O_8$. These effects are particularly apparent for the A_{1g} rotational mode at 265 cm^{-1}. We have given arguments that this phonon strongly perturbs the spin-spin correlations.

ACKNOWLEDGMENTS

We thank N. Kolev for assistance in Raman measurements. This work was supported in part by NSF Grant No. DMR-9804325, the T.L.L. Temple Foundation, the John J. and Rebecca Moores Endowment, and the State of Texas through the Texas Center for Superconductivity at the University of Houston; and at Lawrence Berkeley Laboratory by the Director, Office of Energy Research, Office of Basic Energy Science, Division of Material Sciences of the U.S. Department of Energy under Contract No. DE-AC03-76SF00098. J.B. acknowledges financial support from the Swedish Superconductivity Consortium.

[1] J.L. Tallon, C. Bernhard, M.E. Bowden, P.W. Gilberd, T.M. Stoto, and D.J. Pringle, IEEE Trans. Appl. Supercond. **9**, 1696 (1999).
[2] C. Bernhard, J.L. Tallon, Ch. Niedermayer, Th. Blasius, A. Golnik, E. Brücher, R.K. Kremer, D.R. Noakes, C.E. Stronach, and E.J. Ansaldo, Phys. Rev. B **59**, 14 099 (1999).
[3] O. Chmaissem, J.D. Jorgensen, H. Shaked, P. Dollar, and J.L. Tallon, Phys. Rev. B **61**, 6401 (2000).
[4] J.W. Lynn, B. Keimer, C. Ulrich, C. Bernhard, and J.L. Tallon, Phys. Rev. B **61**, 14 964 (2000).
[5] C.W. Chu, Y.Y. Xue, S. Tsui, J. Cmaidalka, A.K. Heilman, B. Lorenz, and R.L. Meng, Physica C **335**, 231 (2000).
[6] V.G. Hadjiev, A. Fainstein, P. Etchegoin, H.J. Trodahl, C. Bernhard, M. Cardona, and J.L. Tallon, Phys. Status Solidi B **211**, R5 (1999).
[7] A. Fainstein, P. Etchegoin, H.J. Trodahl, and J.L. Tallon, Phys. Rev. B **61**, 15 468 (2000).
[8] V.G. Hadjiev, C. Bernhard, C.T. Lin, T. Ruf, M. Cardona, and J.L. Tallon, Physica C **341-348**, 2255 (2000).
[9] M.N. Iliev, A.P. Litvinchuk, V.N. Popov, R.L. Meng, L.M. Dezaneti, and C.W. Chu, Physica C **341-348**, 2209 (2000).
[10] A.C. McLaughlin, W. Zhou, J.P. Attfield, A.N. Fitch, and J.L. Tallon, Phys. Rev. B **60**, 7512 (1999).
[11] D.J. Pringle, J.L. Tallon, B.G. Walker, and H.J. Trodahl, Phys. Rev. B **59**, R11 679 (1999).
[12] M. Vybornov, W. Perthold, H. Michor, T. Holubar, G. Hilscher, P. Rogl, P. Fischer, and M. Davis, Phys. Rev. B **52**, 1389 (1995).
[13] I. Felner, U. Asaf, S. Reich, and Y. Tsabba, Physica C **311**, 163 (1999).
[14] V.N. Popov, J. Phys.: Condens. Matter **7**, 1625 (1995).
[15] H.J. Rosen, R.M. Macfarlane, E.M. Engler, V.Y. Lee, and R.D. Jacowitz, Phys. Rev. B **38**, 2460 (1988).
[16] Y.K. Atanassova, V.G. Hadjiev, P. Karen, and A. Kjekshus Phys. Rev. B **50**, 586 (1994).
[17] A.P. Fleury and R. Loudon, Phys. Rev. **166**, 514 (1968).
[18] E.F. Steigmeier and G. Harbeke, Phys. Kondens. Mater. **12**, 1 (1970).
[19] N. Suzuki and H. Kamimura, J. Phys. Soc. Jpn. **35**, 985 (1973).
[20] K. Nakamura, K.T. Park, J. Freeman, and J.D. Jorgensen, Phys. Rev. B **63**, 024507 (2001).
[21] R. Weht, A.B. Shick, and W.E. Pickett, in *High Temperature Superconductivity*, edited by Stewart E. Barnes, Joseph Ashkenazi, Joshua L. Cohn, and Fulin Zuo, AIP Conf. Proc. No. 483, (AIP, Woodbury, NY, 1999), p. 141.
[22] R. Matzdorf, Z. Fang, Ismail, J. Zhang, T. Kamura, Y. Tokura, K. Terakura, and E.W. Plummer, Science **289**, 746 (2000).
[23] I.I. Mazin and D.J. Singh, Phys. Rev. B **56**, 2556 (1997).
[24] I. B. Bersuker, *Electronic Structure and Properties of Transition Metal Compounds* (Wiley, New York, 1996).
[25] V. G. Hadjiev (unpublished).
[26] E.T. Heyen, S.N. Rashkeev, I.I. Mazin, O.K. Andersen, R. Liu, M. Cardona, and O. Jepsen, Phys. Rev. Lett. **65**, 3048 (1990).